Cross-borehole electrical monitoring in groundwater remediation projects: understanding the flow path of remediation agents

L. Lévy[1], T. Bording[3], A. Vest Christiansen[1], R. Thalund-Hansen[2], P.L. Bjerg[2]

[1] Hydrogeophysics Group, Department of Geosciences, Aarhus University; [2] Technical University of Denmark, Department of Environmental Engineering; [3] Aarhus Geoinstruments

Summary

In-situ remediation of contaminated groundwater often relies on the installation of a treatment zone degrading the pollution plume. In such projects, adequate delivery of remediation agents in the whole target volume is not trivial. Monitoring the spatial distribution of injected reagents is important for engineers and decision-makers, in order to determine the need of more careful injection in some areas. In this study, we use cross-borehole electrical resistivity tomography (XB-ERT) at two contaminated sites in Denmark to visualize the progressive spreading of two different chemical reagents: an oxidant and a reduction agent made of solid iron particles. Both reagents lead to significant electrical resistivity changes in the subsurface. We observe major differences in the spreading uniformity at the two sites, which we explain by different average permeability and reagent viscosity. We compare tomography results to induction logs in order to evaluate the reliability of the cross-borehole technique.

Cross-borehole electrical monitoring in groundwater remediation projects: understanding the flow path of remediation agents

Introduction

At the European scale, a total of 2.8 million contaminated sites was estimated in 2017 (Pérez and Eugenio, 2018). Remediation by excavation is expensive and can lead to a significant carbon footprint. Remediation by *in-situ* groundwater treatment relies on the installation of a treatment zone (TZ) intersecting the contaminant plume. The TZ is installed by injecting reactive agents, such as strong chemical oxidants (Tsitonaki et al., 2010) or micro-scale zero-valent-iron (ZVI) (Xin et al., 2015). Adequate delivery of reagents is a major challenge for *in-situ* remediation. Cross-borehole electrical resistivity tomography (XB-ERT) is well suited for providing spatial and temporal views of the chemical changes in groundwater, initiated by the injection of chemical remediation agents, while maintaining a high resolution (e.g. Perri et al., 2012). We explore here the lessons learnt from monitoring by XB-ERT the injection of two types of reagents at two sites in Denmark.

Kærgård and Farum study sites

Kærgård Plantation, located near the west coast, is one of the largest polluted sites in Denmark, with over 300.000 tons of pharmaceutical waste (mostly chlorinated solvents) dumped in sand dunes between 1956 and 1973. A clean-up experiment, involving over 100 wells for injection of H_2O_2 (remediation by chemical oxidation) and 30 electrode-boreholes for monitoring, was carried out in December 2019 (Fig. 1). The top eight meters below ground surface are monitored, where the geology consists of sand and gravel layers.

Farum study site is located on a paved parking lot in the suburb of Copenhagen. Waste from a packaging and plastic factory active in the period 1959-1989, led to several groundwater contamination hotspots (chlorinated solvents and hydrocarbons). The chemical reduction agent Provect-IR®, which contains micro-scale ZVI, is the main reagent at this site. Two separate injection rounds were carried out in the same volume in August 2019 and December 2020. XB-ERT monitoring for both injection rounds was carried out with the same nine electrode boreholes (E1-E9, see Fig. 1). The investigated volume is entirely below water table, starting 10 m below ground surface. Geology consists of quaternary sandy till in the top 3-5 m of the investigated volume, underlain by glacio-fluvial meltwater sands.

Cross-borehole ERT set-up and visualization

Three types of electrode configurations are used: (i) "single borehole", with the four electrodes in one borehole, (ii) "AB-MN", with the current dipole in one borehole and the voltage dipole in another one and (iii) "AM-BN", with current sent between two boreholes and voltage measured between the two same boreholes (Bing and Greenhalgh, 2001). Each electrode borehole consists of 32 ring electrodes mounted on a PVC tube. The distance between neighbouring boreholes is 5 and 2.5 m, in Kægård and Farum, respectively, while the corresponding vertical electrode spacing is 0.25 and 0.3 cm. Full-waveform ERT and Time Domain Induced Polarization (IP) data were collected with a 12-channel ABEM Terrameter LS instrument, at a sampling rate of 3750 Hz, with 2 s on-time. More details about data processing and inversion settings can be found in Bording et al. (2021) and Lévy et al. (2021).

In order to provide a meaningful visualisation of the spreading, we plot the ratio of resistivity models obtained after injection, against resistivity models in the baseline. In Kærgård, baseline data were collected in November 2019 while the monitoring data were collected over the three weeks of injection in December 2019. In Farum, a baseline was measured before the first injection "Inj#1", and monitoring took place at +1 day, +14 days, + 90 days, +270 days and +450 days after the end of Inj#1. The second injection, "Inj#2", was monitored thanks to a new baseline and a post-injection round at +20 days.

Two sites, two stories

The difference in spreading of remediation agent, as imaged by XB-ERT, is striking (Fig. 1). In Kærgård, a large low-resistivity anomaly always surrounds the injection screens. A minimum of 30% resistivity drop is observed in transect E18-E19, a few hours after injection in screens nearby. In most transects (e.g. E13-E14 and E20-E25 in Fig. 1), we observe resistivity decrease beyond two orders of

magnitude. Spreading seems to be achieved by both local injection and "natural" flow from upstream. For example, the resistivity decrease below injection screens observed the day of injection in transect E13-E14 is attributed to reagent injected in upstream wells (deeper screens and gravity sinking).
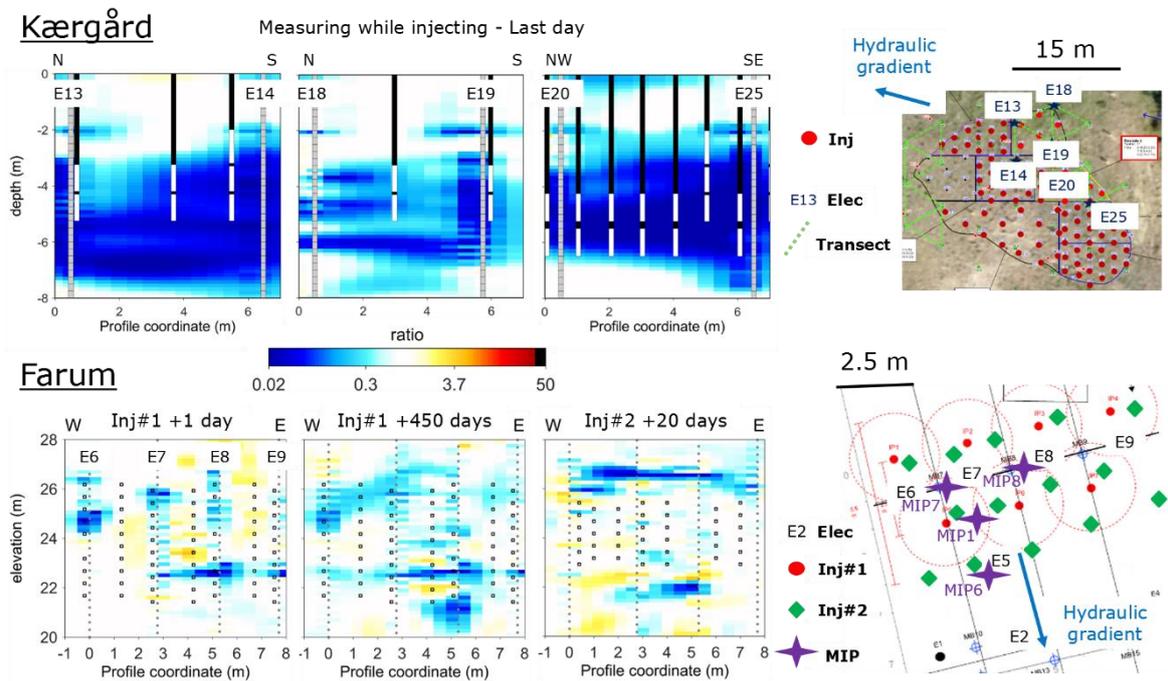

Figure 1. *Ratio plots of resistivity inversions at Kærgård and Farum. The same colour scale is used for all plots: white = no change; light blue = resistivity decrease by 33%; dark blue = resistivity decrease by a factor 50 and beyond. Kærgård: three different transects, including two boreholes each, measured the last day of injection and plotted as the ratio against the baseline. Black bars with white rectangles indicate injection wells and corresponding screens. Grey bars covering represent electrode boreholes. Farum: transect E6-E7-E8-E9 at +1 and +450 days after the first injection, as well as + 20 days after the second injection, plotted as the ratio against the relevant baseline. Injection screen are shown as black points on the transect. On the map, injection wells are shown in red and green for Inj#1 and Inj#2, respectively. Four MIP wells, where induction logs were collected, are also shown.*

In Farum, the injected remediation agent seems to flow through preferential pathways rather than spreading smoothly. Three main clusters, more or less elongated, show a resistivity drop beyond two orders of magnitude one day after Inj#1, at 22.5, 24.5 and 26 m elevation, although injection has taken place in screens covering the whole depth range 21-26 m (Fig. 1). XB-ERT monitoring over 1.5 year after Inj#1 indicates a slow downstream spreading of the low-resistivity anomaly. But the volume between 22.5 and 24.5 m elevation seems to remain mostly empty of remediation agent. Massive upstream and surface leakage, observed during field activities and in chemical monitoring, indicate that the non-uniformity imaged by XB-ERT is only the "tip of the iceberg" (Lévy et al., 2021).

During the second injection, the injection points were focused on the "problematic" volume (see transect Inj#2 +20 days in Fig. 1). According to XB-ERT results, the second injection also ended up flowing through a preferred pathway at 26m elevation, while most of the target volume remained unaffected.

The monitoring of this second injection round in Farum also included induction logs "MIP", which are compared in Fig. 2 to electrical conductivity inferred from XB-ERT at the relevant vertical models, extracted from the TZ (along E6-E7-E8-E9) and NS (along E7-E5-E2) transects. The MIP results confirm the preferred pathway taken by the conductive body in the TZ. Induction logs in MIP6 show consistent conductivity values with the inversion models in the NS transect. Similarly, two conductivity peaks, measured in MIP7 at 12.5 and 13m depth, match the XB-ERT conductivity increase. However,

significant discrepancies are observed with MIP1 and MIP8. These discrepancies occur in model cells with limited sensitivity, due to their distance to the electrode boreholes (see Fig. 1). In addition, the quality of XB-ERT data collected in this last monitoring campaign had significantly dropped compared to previous campaigns, most likely due to damage to the electrodes during the new injection. Therefore, the model cells in-between boreholes are more strongly influenced by lateral constraints.
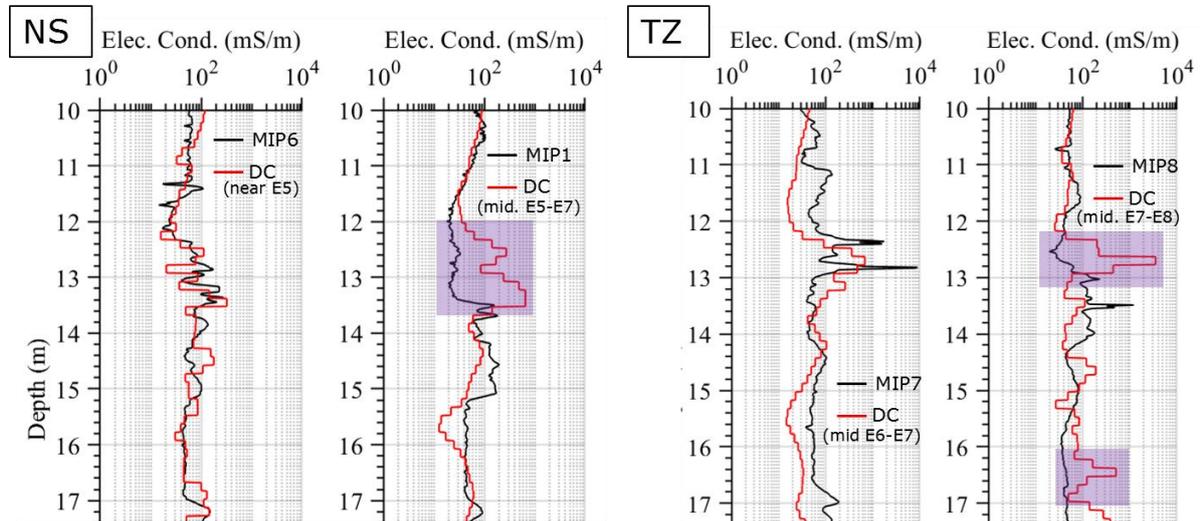

Figure 2. *Comparison of "true" electrical conductivity measured by induction logs (MIP1, MIP6, MIP7 and MIP8, see location in Fig. 1) with inverted conductivity from cross-borehole ERT at Inj#2+20 days in Farum. The depth range 10-20 m corresponds to elevation range 19-29 m.*

How can we explain the differences between Kærgård and Farum?

In order to understand the different spreading patterns at Kærgård and Farum, we computed the permeability field, based on IP data recorded together with ERT and further confirmed at Farum by permeability estimation from 35 grain size analyses at relevant locations (see Lévy et al. (2021)). A major difference between Kærgård and Farum is the average permeability in the main zone targeted by injection: 10^{-9}-10^{-8} m^2 and 10^{-12}-10^{-11} m^2, respectively (Fig. 3). This difference can be explained by the geology: sand/gravel marine deposits versus glacio-fluvial meltwater sand deposits. In addition, the viscosity of the remediation agent is much lower in Kærgård, where H_2O_2 is dissolved in water, than in Farum where micro-scale ZVI particles makes the injected product thicker.

A relevant question is whether the permeability field at Farum, computed using only baseline data, could have helped predict the non-uniform flow path of remediation agent. On Fig. 3, we added a semi-transparent shape on top of the permeability field, showing the distribution of the low-resistivity anomaly at +270 days in the NS transect. We can see that the 2m thick gap around 24m elevation is well within the "high" permeability area. We conclude that the preferential pathway followed by the remediation agent is due to fractures created during the injection at high-pressure. Fracture networks, whether pre-existing or created during injection cannot be imaged by the IP-computed permeability, which mostly takes the size and arrangement of sediment particles into account (Weller et al., 2015). Therefore, the answer to the above question is no.

Conclusions

At both sites, we were able to provide images of the underground reagent distribution along several transects, by comparing the XB-ERT resistivity distributions, before and after injection. The reliability of XB-ERT mapping is validated by comparison to external data, such as induction logs and chemical analyses (not presented here). We note that care should be taken when interpreting model cells in low-sensitivity areas, such as between electrode boreholes, especially when data quality is poor. That limitation in mind, we observe major differences in the spreading uniformity: good uniform spreading

in the target areas at Kærgård versus preferred pathways in Farum, leaving a 2-m thick layer at the centre of the target area almost unchanged.
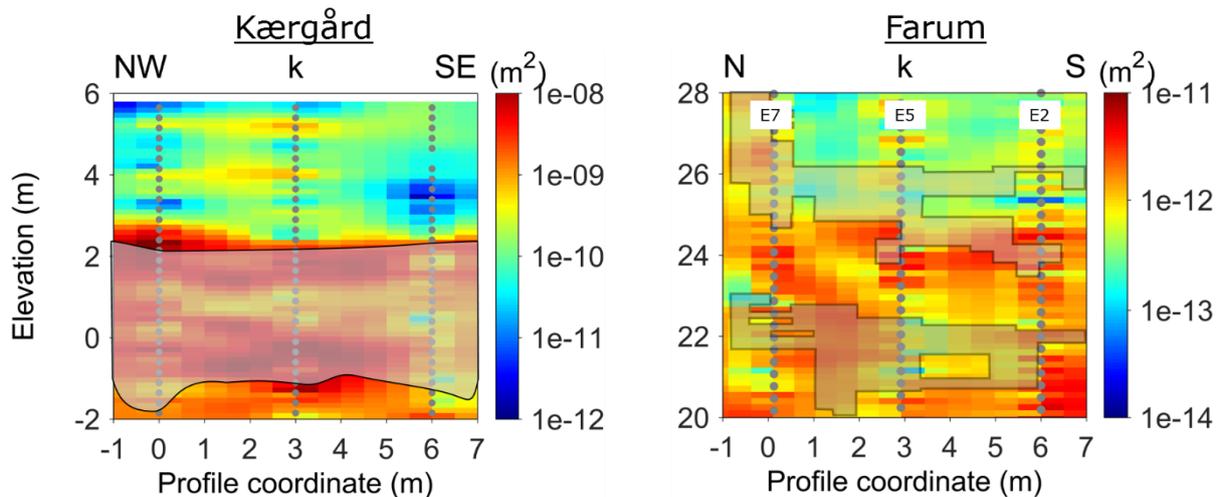

Figure 3. *Permeability models obtained from cross-borehole DCIP inversion at Kærgård (left, published by Bording et al., 2021) and Farum (right). Note the different colour scales. The shaded grey zone indicates the distribution of the low-resistivity anomaly (all cells with a resistivity ratio lower than 0.3) along the profile at +1 day for Kærgård and +270 days for Farum. Electrodes are indicated by grey filled circles.*

Different geology at both sites correspond to an average permeability three decades higher in Kærgård, as predicted by XB-ERT/IP. This helps understand the different spreading. In addition, the injected product in Farum has a much higher viscosity due to the presence of micro-scale zero-valent iron particles. The combination of lower permeability and higher viscosity in Farum were most likely responsible for the creation of ground disturbances during injection. Although pre-existing and potential fractures seem to be the main controlling factor in the flow path in low-permeability-high-viscosity cases like Farum, they remain challenging to predict before-hand by geophysics.

References
Bing, Z., and S. Greenhalgh, 2001, Cross-hole resistivity tomography using different electrode configurations: Geophysical prospecting, **48**, 887-912.
Bording, T., A. K. Kühl, G. Fiandaca, J. F. Christensen, A. V. Christiansen, and E. Auken, 2021, Cross-borehole geoelectrical time-lapse monitoring of in situ chemical oxidation and permeability estimation through induced polarization: Near Surface Geophysics, **2021**, 43-58.
Lévy, L., Thalund-Hansen, R., Bording, T., Fiandaca, G., Christiansen, A.V., Rügge, K., Tuxen, N., Hag, M. and Bjerg, P.L . 2021, Monitoring of a bio-chemical treatment zone installation in the subsurface by means of time-lapse cross-borehole complex electrical tomography: Under Review at Water Resources Research.
Perri, M. T., G. Cassiani, I. Gervasio, R. Deiana, and A. Binley, 2012, A saline tracer test monitored via both surface and cross-borehole electrical resistivity tomography: Comparison of time-lapse results: Journal of Applied Geophysics, **79**, 6-16.
Pérez, A. P., and N. R. Eugenio, 2018, Status of local soil contamination in Europe.
Tsitonaki, A., B. Petri, M. Crimi, H. Mosbæk, R. L. Siegrist, and P. L. Bjerg, 2010, In situ chemical oxidation of contaminated soil and groundwater using persulfate: a review: Critical Reviews in Environmental Science and Technology, **40**, 55-91.
Weller, A., L. Slater, A. Binley, S. Nordsiek, and S. Xu, 2015, Permeability prediction based on induced polarization: Insights from measurements on sandstone and unconsolidated samples spanning a wide permeability range: Geophysics, **80**, D161-D173.
Xin, J., X. Zheng, J. Han, H. Shao, and O. Kolditz, 2015, Remediation of trichloroethylene by xanthan gum-coated microscale zero valent iron (XG-mZVI) in groundwater: effects of geochemical constituents: Chemical Engineering Journal, **271**, 164-172.